Design Procedure and Implementation of Inductor Using Litz Wires for Induction Heating

Chi-Thang Phan-Tan
BAP Power Corporation
d.b.a. Cenergy Power
California, United States
0000-0002-0646-8304

Thuong Ngo-Phi
Ho Chi Minh City University of Technology (HCMUT)
Vietnam National University Ho Chi Minh City
Ho Chi Minh City, Vietnam
ngophithuongbk@gmail.com

Nam Nguyen-Quang*
Ho Chi Minh City University of Technology (HCMUT)
Vietnam National University Ho Chi Minh City
Ho Chi Minh City, Vietnam
*Corresponding: nqnam@hcmut.edu.vn

2023 International Conference on System Science and Engineering (ICSSE) | 979-8-3503-2294-1/23/$31.00 ©2023 IEEE | DOI: 10.1109/ICSSE58758.2023.10227150

***Abstract*—Induction heating (IH) is applied to convert electricity into thermal energy with a high frequency (HF) current flowing through an inductor. Litz wires help mitigate the power loss at the inductor winding in HF applications by reducing eddy currents. This work presents a detailed approach to designing a power inductor using Litz wires for IH using an inductor-inductor-capacitor (LLC) resonant tank. In comparison to a single solid or stranded wire with the same requirements, the developed formulas in this paper show that the size of the Litz wire inductor is approximately 15% smaller. The step-by-step design procedure is presented with all required formulas and associated information. The feasibility of the proposed design process is illustrated and verified through an experiment on a 2 kW, 100 kHz LLC IH system.**

Keywords—Induction heating, LLC, Litz wire, inductor design, winding loss, inductor winding, high frequency

I. INTRODUCTION

Inductors are one of the most essential components in power electronic circuits. Inductors for switching power applications, especially for induction heating (IH), are designed and wound separately to meet a specific frequency and current level. This paper develops formulas for the design of power inductors fabricated using Litz wires as this delivers high performance at high frequency (HF). In power electronic applications at HF, the winding design must target low AC resistance and low eddy currents. Eddy currents in the winding conductor lead to proximity and skin effects that cause inductor losses [1]-[3]. The proximity effect is the dominant conductor loss mechanism at HF [4]. The varying magnetic field of one AC conductor induces eddy currents in the nearby conductors reducing their current carrying capacity and increasing the inductor resistance and power losses. Similar to the proximity effect, the skin effect also causes power losses by the reduction of the conducting area for current.

To handle these issues, Litz wires are considered in the application of HF from 50 kHz to 500 kHz. Litz wire is made of multiple individually insulated wires twisted in a uniform pattern [4]. In IH applications at HF, Litz wires are chosen to reduce inductor copper loss in comparison to solid or stranded wires as presented in [5]-[8]. To reduce power loss in high-frequency applications (from 20 kHz to 800 kHz), Litz wires are used [9]. In addition, the Litz wire is easier to bend in comparison to a large solid conductor. For carrying a large amount of current, several Litz wires are used.

There are existing guides for the design of power inductors and transformers [10], [11]. These are useful for designing the inductor using a single solid round wire for the winding. However detailed formulas for designing inductors using Litz wires are not sufficiently described. There are studies related to the performance of inductors using Litz wires such as winding resistance and thermal effect. In [12], the AC resistance of Litz wire is considered including the fringing effect of the air gap in HF applications. The selection of optimal frequency, window utilization factor, and packing factor for IH using Litz are presented in [13] to lessen the power loss from the copper winding volume. Methods of selecting the wire strand size are presented in [14]-[15] with the consideration of skin depth. In [16], the calculation and comparison of solid-round wires and multi-strand Litz wires of the same cross-sectional conductor area are investigated. The research study demonstrates that the Litz wire performs better than the solid-round wire in a specific frequency range where the winding resistance of the Litz wire is lower than the solid wire.

The formulas in this paper are mainly developed from the single-wire inductor design in [10]. Detailed instructions for inductor design are presented in Section II. The construction and experimental characterization of an inductor to validate the design process are discussed in Section III. In Section IV, the experiment results are conducted to verify the developed formulas and compare the efficiency between the inductor using Litz wire and the inductor using a single-stranded wire. The benefits and assumptions of the design process and an estimate of inductor size are discussed in Section IV and conclusions are drawn in Section V.

II. INDUCTOR DESIGN PROCESS

This paper proposes to use a standard Litz wire structure consisting of seven insulated strand wires twisted together as shown in Fig. 1.

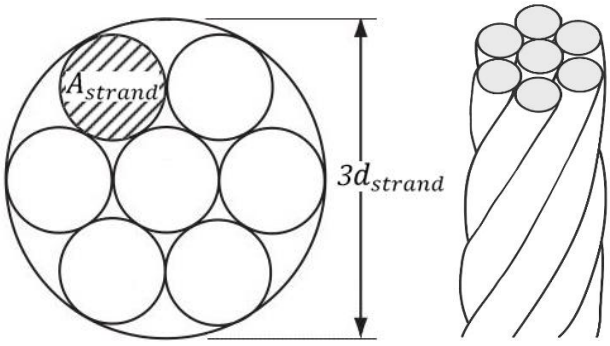

Fig. 1. Seven-strand Litz wire structure.

The structure in Fig. 1 keeps a static circular geometry of the wire, and the twisting form can be achieved by an electric drill without any support from twisting machines. The formulas in this paper are developed with this standard seven-strand Litz wire. Therefore, the application of Litz wire with more than seven strands would not be considered in this research.

The sequence of steps to design an inductor is shown in Fig. 2. There are 11 steps to follow and detailed formulas for each calculation step are presented.

Step 1: Specify the initial values of the needed inductor $\mathrm{L}, f, I_{max}, I_{rms}, T_{max}, \Delta T$

Step 2: Choose a core material corresponding to the frequency. Then specify core parameters and select flux density B_{max}

Step 3: Select a core size with higher area product than A_P

$$A_P = \left(\frac{k_i \mathrm{L} I_{max}^2}{k_t B_{max}} \sqrt{\frac{7(1+\gamma)}{9 k_u \Delta T}} \right)^{\frac{8}{7}} \quad (1)$$

Step 4: Calculate thermal resistance R_θ and maximum dissipation power of the core P_D

$$R_\theta = 0.06/\sqrt{V_c} \quad (2) \qquad P_D = \Delta T / R_\theta \quad (3)$$

Step 5: Calculate the effective relative permeability μ_{e_opt} via the resistivity ρ of winding wires at T_{max}

$$\rho = \rho_0 [1 + \alpha_0 (T_{max} - 20)] \quad (4)$$

$$\mu_{e\_opt} = \frac{B_{max} k_i l_c}{\mu_0} \sqrt{\frac{9 \rho l_{turn}}{7 P_D k_u A_{wd}}} \quad (5)$$

Step 6: Choose the core with an air gap length l_g

$$l_g \le l_c / \mu_{e\_opt} \quad (6)$$

Step 7: Find turns quantity N via induction factor A_L. If A_L is not provided by the core manufacturer, it may be calculated as in (7) where k_g is taken from Table V

$$A_L = \mu_0 A_c \Big/ \left(\frac{l_c}{\mu_r} + \frac{l_g}{k_g} \right) \quad (7) \qquad N = \sqrt{\mathrm{L}/A_L} \quad (8)$$

Step 8: Select diameter of winding wires via skin depth δ

$$\delta = \sqrt{\rho/(\pi f \mu_0)} \quad (9) \qquad d_{strand} = 2\delta \quad (10)$$

Step 9: Calculate the number of Litz wires n_{Litz} to carry the current density J_0

$$J_0 = \frac{k_t}{\sqrt[8]{A_P}} \sqrt{\frac{9 \Delta T}{7 k_u (1+\gamma)}} \quad (11)$$

$$n_{Litz} = \frac{k_i I_{max}}{7 J_0 A_{strand}} \quad (12)$$

Step 10: Calculate the window utilization factor

$$k_{u\_after} = 9 A_{strand} n_{Litz} N / A_{wd} \quad (13)$$

Step 11: Calculate the power loss of the inductor

$$P_{core} = V_c k_{core} f^\alpha (\Delta \mathrm{B}/2)^\beta \quad (14)$$

$$P_{wire} = \frac{\rho N l_{turn} I_{rms}^2}{7 n_{Litz} A_{strand}} \quad (15)$$

$$P_{loss} = P_{wire} + P_{core} \quad (16)$$

Fig. 2. Process of inductor design using Litz wire.

In Step 1, the initial values of the required inductor are specified such as inductance L and current frequency f. The maximum operating temperature is T_{max} and the temperature rise ΔT is estimated by the difference between the ambient temperature and T_{max}. The winding wires must withstand the maximum current I_{max} and the root-mean-square (RMS) current I_{rms}. Then the coefficient k_i is determined as I_{rms}/I_{max}. A complete nomenclature for all variables can be found in Table IV.

The selection of the core material and size is described in Step 2 and Step 3. Soft magnetic materials are chosen for HF applications [10]. There are different core shapes to be selected for the winding so that a common value of A_P helps determine the size of the core. The coefficient k_u is the ratio of the area occupied by the wires to the available area of the core. When winding manually, k_u should be chosen to be 40 to 50% of the core winding area. The specifications of the selected core such as V_c, l_c, A_{wd}, l_{turn}, μ_r, α, β and k_{core} can then be found from the datasheet provided by the manufacturer. Table VI shows typical parameter values of common soft magnetic materials.

The next step is determining the air gap of the inductor. An air gap l_g as shown in Fig. 3 is necessary for storing most of the inductor energy, allowing higher current and yielding an inductance value that is less temperature-dependent than without the air gap [10]. The length of the air gap is determined through the optimal effective relative permeability μ_{e_opt} as described from Step 4 to Step 6.

The number of turns N is calculated for the needed inductance L via the induction factor A_L in Step 7. The value of A_L can be found in the core datasheet with a specific air gap length. In the case that the chosen air gap l_g is not listed in the datasheet, it may be calculated as in (7) with k_g from Table V.

Because of the skin effect which pushes the current to flow near the surface of the conductor, the strand wire size is selected from the skin depth to utilize the effective area of the conducting area. As in Step 8, the diameter d_{strand} of the stranded wires is chosen to be twice the skin depth δ [4]. The chosen strand wire size may not carry the needed current capacity so more than one Litz wire might be used. The number of Litz wires n_{Litz} is then calculated through current density J_0 as described in Step 9.

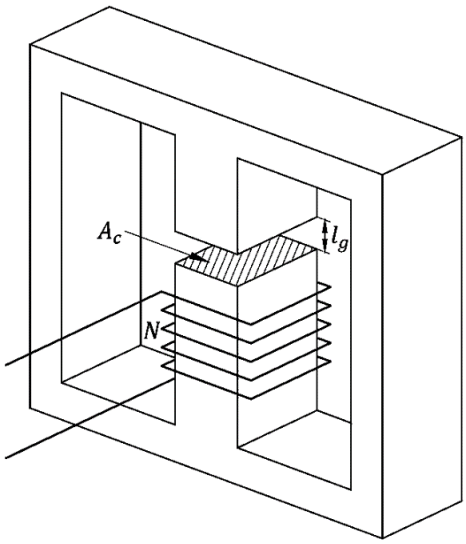

Fig. 3. A basic E-core inductor with an air gap l_g.

With the chosen strand wire size d_{strand} and n_{Litz}, the fill ratio of the Litz wires to the core winding area is calculated as in Step 10. The power losses of the inductor will then be estimated as in Step 11.

The next section is an example of how these design steps are applied to meet a specific inductor design requirement.

III. Design Example

An inductor is constructed to verify the theoretical formulas presented in Section II. The inductor L_s is to be designed with an inductance of 2.48 µH for an LLC resonant tank as shown in Fig. 4a [17]. The LLC resonant inverter is supplied by a 3-phase bridge rectifier and an LC filter. The H-bridge inverter provides resonant current through a DC-blocking capacitor C_b and a matching transformer Tr. The LLC resonant circuit is on the transformer secondary side. It includes a series inductor L_s, a parallel capacitor C, and a work-head inductor L_{IH}. The simulated current passing through L_s is shown in Fig. 4b.

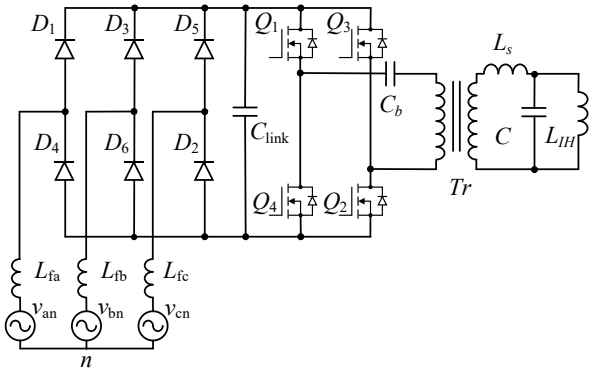

a. LLC induction heating circuit

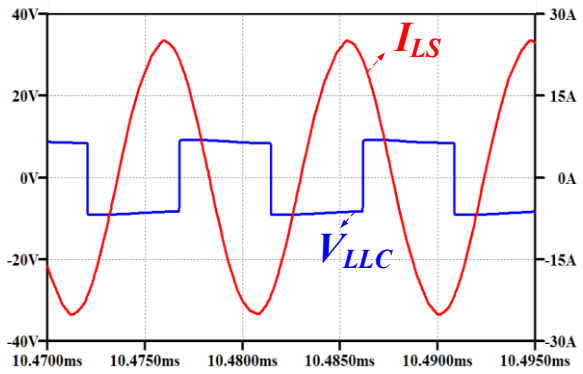

b. Simulated current and voltage of the LLC induction heating circuit

Fig. 4. LLC induction heating circuit and simulated filter inductor current.

The requirements of the inductor and the IH circuit are shown in Table I.

TABLE I. Design Specifications

Parameter	Value	Unit
Inductance L_s	2.48	µH
RMS L_s current I_{rms}	17.7	A
Frequency $f = 1/T$	100	kHz
Maximum temperature T_{max}	60	°C
Temperature rise ΔT	40	°C

Step 1: As seen in Table I, the current I_{rms} is 17.7 A. The maximum current I_{max} is calculated to be 25 A. Then the parameter k_i is calculated as the following:

$$k_i = I_{rms}/I_{max} = 0.707 \quad (20)$$

Step 2: With the frequency requirement of 100 kHz, the N87 ferrite material is chosen for the inductor core, and its parameters are shown in Table II. This material is chosen because it applies to frequencies from 25 kHz to 500 kHz [18]. More soft magnetic materials can be found in Table VI. The maximum flux density B_{max} is chosen as 0.4 T or the saturation flux density B_{sat}.

TABLE II. Specifications of Ferrite N87 [10]

Parameter	Value	Unit
Saturation flux density B_{sat}	0.4	T
Material parameter k_{core}	16.9	1
Material parameter α	1.25	1
Material parameter β	2.35	1

Step 3: The inductor is wound manually so that the window utilization factor k_u is chosen as 50% of the core's winding area. With negligible flux ripple, the coefficient γ is selected to be zero or it is assumed that the core losses P_{core} are negligible in comparison to the wire losses P_{wire} [10]. The parameters k_t is taken with its typical value of 48,200 as in Table IV. From (1), A_P is calculated as 0.2 cm^4. The core ETD49 is used for its availability and its specifications are presented in Table III.

TABLE III. Specifications of ETD49 Core [19]

Parameter	Value	Unit
Window area of core for winding A_{wd}	2.75	cm^2
Cross-sectional area of the core A_c	2.11	cm^2
Product area A_P ($A_P = A_c \times A_{wd}$)	5.80	cm^4
Mean length of a turn l_{turn}	8.7	cm
Volume of the core V_c	24.1	cm^3
Effective magnetic path length l_c	11.4	cm
Relative permeability of the core μ_r	1630	1

Step 4: From (2) and (3), the value of thermal resistance R_θ is determined as 8.39 °C/W and the maximum dissipation power of the core P_D is 4.77 W.

Step 5: The material of the selected winding wires is copper whose parameters of ρ_0 and α_0 are shown in Table IV. From (4), the resistivity ρ of the copper wires at T_{max} is calculated as (2.00×10^{-8}) Ωm. The optimum effective relative permeability μ_{e_opt} is then calculated as 25.46.

Step 6: With a known μ_{e_opt}, the air gap l_g should be less than 5.46 mm. Then select the air gap length l_g to be 5 mm.

Step 7: The datasheet of the core does not show the value of A_L for a gap of 5 mm. From Table V, the value of k_g is calculated using a linear interpolation as 1.95 and the induction factor A_L is determined as 0.174 nH. As in (8), the number of turns is calculated as 3.8. Choose $N = 4$ turns.

Step 8: The calculated skin depth δ is 0.23 mm. Choose d_{strand} to be 0.3 mm with cross-sectional area A_{strand} is 0.0707 mm^2.

Step 9: From (11), the current density J_0 is calculated as 3.46 A/mm^2 then the suggested number of Litz wires is 10.32. Choose $n_{Litz} = 10$.

Step 10: With the selected Litz wire size and quantity, the fill area of the wires in comparison to the core window is then determined $k_{u\_after} = 6\%$.

Step 11: As in (15), the wire loss P_{wire} is 0.54 W. The flux density ripple ΔB is taken to be 0.4 T. The core loss is determined from (14) as 35.04 W. The total wire and core losses P_{loss} is 35.58 W. The losses are calculated in the most extreme condition so that in practical operation the inductor may dissipate less than the calculated value of power.

IV. Experimental Result and Discussion

The implemented inductor with 10 Litz wires and 4 turns on the ETD49 core is shown in Fig. 5a. The L_s inductance value measured by the LCR meter at 100 kHz is 2.47 µH which is very close to the desired value of 2.48 µH.

a. Using Litz wires b. Using 145-strand wire

Fig. 5. Measurement of the implemented inductors

The experimental current of the output inductor L_s is shown in Fig. 6, with current ripples at zero crossing of the input voltage applied to the LLC tank, and at input voltage distortion points due to magnetizing current of the coupling transformer. In comparison to the simulated results in Fig. 4, the experiment in Fig. 6 verifies the developed formulas in Section II.

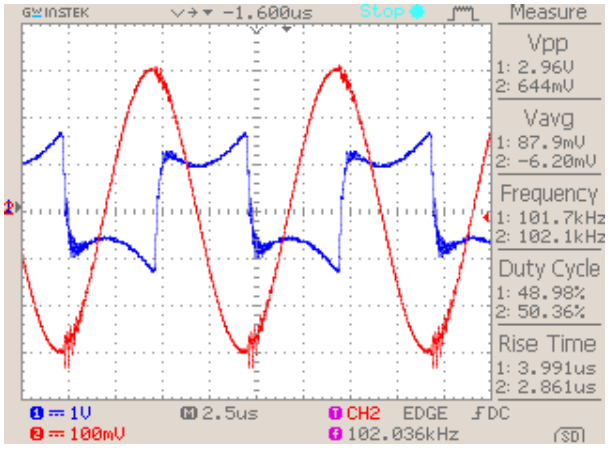

Fig. 6. Measured current and voltage of the LLC induction heating circuit

For power loss comparison between Litz wire and normal stranded wire, another inductor is made using a 145-strand wire with a diameter of 0.2 mm for each strand. The stranded wire inductor also has 4 turns of winding and a 5-mm air gap. The measured inductance value of the stranded wire inductor is 2.44 µH as shown in Fig. 5b.

A size comparison is now conducted. As in [10], the formula for calculating the product area A_{P_single} for the inductor using single-strand wire is shown below.

$$A_{P\_single} = \left(\frac{k_i L I_{max}^2}{k_t B_{max}} \sqrt{\frac{1+\gamma}{k_u \Delta T}} \right)^{8/7} \tag{23}$$

The values of A_{P_single} is then compared to the product area A_{P_Litz} in (1) as the following.

$$\frac{A_{P\_Litz}}{A_{P\_single}} = \left(\sqrt{7/9} \right)^{8/7} = 86.6\% \tag{24}$$

It can be concluded that the core size of the Litz wires is only 87% in comparison to the single-strand inductor. In other words, the inductor size using single-strand wire is 15% larger than the inductor size using Litz wire.

V. Conclusion

A comprehensive design procedure to calculate the essential parameters for a Litz-wire inductor has been presented. This calculation method can be flexibly applied to any specification of inductors and the availability of hardware. The formulas and steps are summarized and presented for a practical power inductor. Unnecessary parameters and formulas that are also involved in the process of inductor design but have negligible effects are considered to be filtered out without losing the accuracy of the calculation. The guidance in this paper is presented accompanied by theoretical values and parameters of commonly available materials. An example design has been conducted following the presented step-by-step instructions to construct the series inductor for an LLC resonant circuit.

Experimental measurements on the constructed inductor have confirmed the presented formulas. It has been theoretically proven that the size of the Litz wire inductor is reduced by approximately 15% in comparison to the single solid wire winding inductor.

Appendix

TABLE IV. Nomenclature

Label	Description	Unit
A_c	cross-sectional area of the core	m^2
A_L	induction factor	H
A_t	surface area of the core	m^2
A_P	product of A_c and A_{wd} ($A_P = A_c \times A_{wd}$)	m^4
A_{strand}	cross-sectional area of strand wire	m^2
A_{wd}	window area of core for winding	m^2
B_{max}	maximum flux density (typical $B_{max} \approx (0.6-0.7)B_{sat}$)	T
B_{sat}	saturation flux density	T
ΔB	flux density ripple	T
d_{strand}	strand wire diameter	m
f	frequency of current	Hz
N	number of turns of inductor	1
n_{Litz}	number of Litz wires of inductor	1
h_c	heat transfer coefficient (typical $h_c = 10$)	W/m^2 °C
I_{max}	maximum current of inductor	A
I_{rms}	RMS of inductor current	A
J_0	current density	A/m^2
k_a	coefficient; $k_a = A_t/A_P^{1/2}$ (typical $k_a = 40$)	1
k_{core}	material parameter (N87 material $k_c = 16.9$)	1
k_i	current coefficient; $k_i = I_{rms}/I_{max}$	1
k_g	air gap correction coefficient	1
k_t	coefficient; $k_t = \sqrt{(h_c k_a)/(\rho k_w)}$ (typical $k_t = 48.2 \times 10^3$)	(A^2/m^3 °C)$^{1/2}$
k_u	window utilization factor	1
k_w	coefficient; $k_w = V_w/A_P^{3/4}$ (typical $k_w = 10$)	1

L	needed inductance	H
l_c	effective magnetic path length	m
l_g	length of the air gap	m
l_{turn}	mean length of a turn (MLT) of winding wires	m
P_{core}	power loss of the core	W
P_D	maximum dissipation power of the core	W
P_{loss}	total power loss of the inductor	W
P_{wire}	power loss of the winding wire	W
R_θ	thermal resistance of the core	℃/W
T_{max}	maximum temperature; $T_{max} = T + \Delta T$	℃
ΔT	temperature rise	℃
V_c	volume of core	m^3
V_w	volume of winding	m^3
α	material parameter (N87 material $\alpha = 1.25$)	1
α_0	temperature coefficient of resistivity at 20 ℃ ($\alpha_{0\_cu} = 0.004$)	1/℃
β	material parameter (N87 material $\beta = 2.35$)	1
γ	coefficient; $\gamma = P_{core}/P_{wire}$	1
δ	skin depth	m
μ_0	magnetic permeability of free space ($\mu_0 = 4\pi \times 10^{-7}$)	H/m
μ_r	relative permeability	1
μ_{e_opt}	optimum effective relative permeability	1
ρ	resistivity of conductor	Ωm
ρ_0	resistivity of conductor at 20 ℃ ($\rho_{0\_cu} = 1.72 \times 10^{-8}$)	Ωm

TABLE V. VALUES OF THE AIR GAP CORRECTION [19]

l_g (mm)	0.1	0.2	0.5	1.0	2.0	3.0	4.0
k_g	1.1	1.2	1.3	1.4	1.5	1.65	1.8

TABLE VI. TYPICAL SOFT MAGNETIC MATERIALS [10]

Material	**Model**	B_{sat} **(T)**	k_{core}	α	β
Ferrite	Epos N87	0.4	16.9	1.25	2.35
Nanocrystalline	Viroperm 500F	1.2	2.3	1.32	2.1
Amorphous	Metglas 2605	1.56	0.053	1.81	1.74
Si iron	Unisil 23M3	2.0	3.388	1.70	1.90
Ni-Fe	Permalloy 80	0.82	0.448	1.56	1.89
Powdered iron	Micrometals 75μ	0.95	1798	1.02	1.89

ACKNOWLEDGMENT

We acknowledge Ho Chi Minh City University of Technology (HCMUT), VNU-HCM for supporting this study.

REFERENCES

[1] P. L. Dowell, “Effects of eddy currents in transformer windings,” *Proceedings of the Institution of Electrical Engineers*, vol. 113, no. 8, p. 1387, 1966.

[2] J. Acero, I. Lope, J. M. Burdío, C. Carretero and R. Alonso, “Loss analysis of multistranded twisted wires by using 3D-FEA simulation,” *2014 IEEE 15th Workshop on Control and Modeling for Power Electronics (COMPEL)*, Santander, 2014, pp. 1-6, doi: 10.1109/COMPEL.2014.6877168.

[3] C. R. Sullivan and R. Y. Zhang, “Analytical model for effects of twisting on litz-wire losses,” *2014 IEEE 15th Workshop on Control and Modeling for Power Electronics (COMPEL)*, Santander, 2014, pp. 1-10, doi: 10.1109/COMPEL.2014.6877187.

[4] C. W. T. McLyman, Transformer and Inductor Design Handbook, CRC Press, 2011.

[5] M. Hataya, Y. Oka, K. Umetani, E. Hiraki, T. Hirokawa, and M. Imai, “Novel thin heating coil structure with reduced copper loss for high frequency induction cookers,” in Proc. IEEE Intl. Conf. Elect. Mach. Syst.,Nov. 2016, pp. 1–6.

[6] J. Acero, P. J. Hernández, J. M. Burdío, R. Alonso, and L. A. Barragán, “Simple resistance calculation in Litz-wire planar windings for induction cooking appliances,” IEEE Trans. Magn., vol. 41, no. 4, pp. 1280–1288, April. 2005.

[7] K. Paul, "ZVZCS SRI Guides Optimal Use of Copper and Core for Air-Cooled Nanocrystalline Transformer for Induction Heating," in IEEE Transactions on Industry Applications, vol. 56, no. 2, pp. 970-978, March-April 2020, doi: 10.1109/TIA.2020.2967329.

[8] S. Kawahara, K. Umetani, M. Ishihara and E. Hiraki, "Frequency Dependence Deterioration of AC Resistance in Large-Diameter Litz Wire for High Power Induction Heating," 2022 IEEE Energy Conversion Congress and Exposition (ECCE), Detroit, MI, USA, 2022, pp. 1-7, doi: 10.1109/ECCE50734.2022.9948072.

[9] A. Reatti and F. Grasso, "Solid and Litz-wire winding non-linear resistance comparison," *Proceedings of the 43rd IEEE Midwest Symposium on Circuits and Systems (Cat.No.CH37144)*, Lansing, MI, USA, 2000, pp. 466-469 vol.1, doi: 10.1109/MWSCAS.2000.951684.

[10] W. G. Hurley, W. H. Wolfle, Transformers and Inductors for Power Electronics: Theory, Design and Applications, Wiley, 2014.

[11] A. Van den Bossche, V. C. Valchev, Inductors and Transformers for Power Electronics, CRC Press, 2005, doi: 10.1201/9781420027280.

[12] A. Stadler and C. Gulden, “Copper losses of litz-wire windings due to an air gap,” *2013 15th European Conference on Power Electronics and Applications (EPE)*, Lille, 2013, pp. 1-7, doi: 10.1109/EPE.2013.6631820.

[13] I. Lope, J. Acero and C. Carretero, "Analysis and Optimization of the Efficiency of Induction Heating Applications With Litz-Wire Planar and Solenoidal Coils," in IEEE Transactions on Power Electronics, vol. 31, no. 7, pp. 5089-5101, July 2016, doi: 10.1109/TPEL.2015.2478075.

[14] C. R. Sullivan, “Optimal choice for number of strands in a litz-wire transformer winding,” in *IEEE Transactions on Power Electronics*, vol. 14, no. 2, pp. 283-291, March 1999, doi: 10.1109/63.750181.

[15] C. R. Sullivan and R. Y. Zhang, “Simplified design method for litz wire,” *2014 IEEE Applied Power Electronics Conference and Exposition - APEC 2014*, Fort Worth, TX, 2014, pp. 2667-2674, doi: 10.1109/APEC.2014.6803681.

[16] R. P. Wojda and M. K. Kazimierczuk, “Winding resistance of litz-wire and multi-strand inductors,” in *IET Power Electronics*, vol. 5, no. 2, pp. 257-268, Feb. 2012, doi: 10.1049/iet-pel.2010.0359.

[17] Thuong Ngo-Phi., & Nam Nguyen-Quang. (2021). LLC Inverter Design Procedure for Induction Heating with Quantitative Analysis of Power Transfer. VNUHCM Journal of Engineering and Technology, 4(1), 739-747.

[18] TDK, “Ferrites and accessories SIFERRIT material N87,” datasheet, 2017.

[19] TDK, “ETD49/25/16 Core and accessories,” datasheet, 2013.

[20] MMG, “Soft Ferrite Materials & Components for Power, Signal and EMC Applications,” datasheet, pp. 176.